Laser Spectroscopic Trace-Gas Sensor Networks for Atmospheric Monitoring Applications

Stephen So
Princeton University
B321 EQuad
Princeton, NJ 08540
609-258-8948
sso@princeton.edu

Ardalan Amiri Sani, Lin Zhong, Frank Tittel
Rice University
6100 S. Main St. MS366
Houston, TX 77005
713-348-4833
{aa15, lzhong, fkt}@rice.edu

Gerard Wysocki
Princeton University
B321 EQuad
Princeton, NJ 08540
609-258-8187
gwysocki@princeton.edu

ABSTRACT

Laser-based atmospheric trace-gas sensors have great potential for long-term, real-time, maintenance free environmental monitoring in distributed Wireless Sensor Networks (WSN). We are developing a laser based chemical sensing technology with wide-area autonomous wireless sensor networking as the final target. Our prototype sensor measures atmospheric oxygen concentration in the form of a battery powered, handheld unit with power consumption <0.3W, sensitivity of 0.02% in 1 sec, weight of <0.4kg without batteries, low cost, high specificity, and the robustness required for long term sensing applications. We demonstrate gas plume localization and quantification using a prototype three-node sensor network. The technology is modular and can be used for different environmentally important molecules such as CO_2, NOx, and methane with exceptionally high specificity.

Categories and Subject Descriptors

C.3 **[Special-Purpose and Application-Based Systems]** *Real-time and embedded systems* • J.2 **[Physical Sciences and Engineering]** *Earth and atmospheric sciences*

General Terms

Measurement, Performance, Design, Experimentation

Keywords

Laser Spectroscopy, Trace-Gas Sensing, Sensor Networks, Plume Detection

1. INTRODUCTION

Trace-gas sensing has been difficult to implement with an adequate sensitivity, size, power consumption, and cost suitable for distributed real-time environmental sensor networks. A number of methods such as gas chromatography, mass spectrometry, and Fourier transform infrared spectroscopy provide the sensitivity and specificity required for environmental sensing, but typically have considerable tradeoffs between size, cost, and power consumption vs. performance, robustness, simplicity, and autonomy. Electrochemical sensors can fulfill size and cost requirements, but their sensitivity and, more importantly, specificity is often inadequate for many environmental sensing applications. Methods which require frequent calibration with reference gases are undesirable in field deployments, since consumables are not easily replaced. Laser spectroscopy provides a sensor which is capable of self-calibration, can achieve part-per-million to part-per-trillion concentration sensitivities, in a robust, compact, autonomous, low cost package.

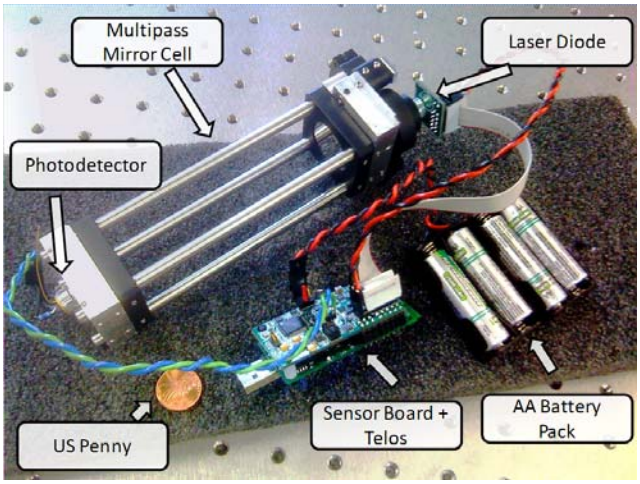

Figure 1: Photograph of a complete battery operated wireless sensor for O_2 equipped with a Telos WSN module. The sensor can be operated continuously on 4 rechargeable AA batteries for 16 hours.

Several important issues exist in regards to direct integration of laser based sensors into sensor networks which we addressed previously in Ref. [23]. We have significantly improved our platform in terms of the following:

ESSA Workshop '09, April 16, 2009, San Francisco, California, USA

1) Optimized algorithms, software and hardware have been implemented, which allowed for significant improvements in terms of accuracy and precision as well as for more effective utilization of the available computation resources of the microcontroller.

2) We achieved significant improvements in terms of total power consumption requiring <0.3W including the laser, temperature control, and wireless transmission. These sensors are intended to be deployed with batteries. This would be difficult with other available instrumentation platforms suitable for laser spectroscopy [12, 27, 30] since power consumption typically ranged from >3W-1kW.

3)We have implemented custom optics and opto-mechanical construction to achieve a lightweight, robust, and compact footprint which matches WSN modules. This allows deployment anywhere without the high cost of designing and developing a dedicated infrastructure.

4)We optimized the cost and made the design replicable, as spatial resolution for real-time mapping of gas concentration data is directly dependent on node density. To-date, laser based sensors have required >$20k+ for research platforms, mostly custom manufactured for ultra-high sensitivity. In contrast, our platform uses mostly off-the-shelf, high volume, low cost components.

Figure 1 shows the complete sensor we have developed for networked trace-gas sensing. We will describe the improvements we have made to our embedded systems (see Figure 2) in order to lower power consumption while increasing performance, especially in regards to a digital lock-in amplifier designed specifically for compact, low cost, and low power, while still maintaining performance comparable to standalone laboratory instrumentation.

In this work, we specifically address: 1) development of high efficiency code, which enables low power methodologies allowing maximum processor sleep mode time, and 2) improvement of sensor stability to avoid any post-processing and data corrections.

We furthermore demonstrate a WSN deployment of a three node network measuring oxygen in the atmosphere, with an example detection of a plume released from a gas cylinder.

2. MOTIVATION

2.1 Applications

Trace-gas sensors based on laser spectroscopy find use in environmental, industrial, and security applications. Environmental sensors for methane, CO_2, carbon monoxide, and water vapor [17, 31, 32] currently provide scientifically valuable data for atmospheric carbon cycle and greenhouse effects. Other sensors that perform measurements of molecules important for atmospheric chemistry such as formaldehyde [13] or nitric oxide [33] have also demonstrated very high sensitivities and deliver important data. Various industries have implemented laser

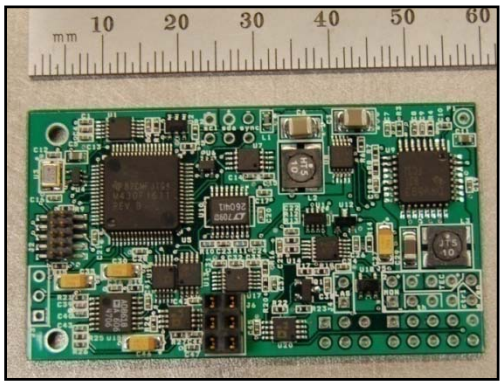

Figure 2: Real-time embedded systems based on MSP430 developed for laser based spectroscopic trace-gas sensing.

spectroscopic chemical sensing for monitoring applications such as natural gas leak detection in the oil and gas industry [29]. There has been significant research towards security applications e.g. for detection of explosives and chemical warfare agents [28], or in space exploration science e.g. spectroscopic sensors installed on Mars rovers [7, 30].

Chemical sensing is infrequently implemented in sensor networks, mainly due to the size, cost, and complexity of useful chemical sensors. Additionally, few sensors implemented into sensor networks have required high precision control, acquisition, and processing [1], which makes the adaptation of available gas sensing technology into sensor networks difficult.

2.2 Impact on Environmental Sensing

Sensor networks allow for acquisition of spatially resolved long-term real-time data which is not possible with other types of sensing technologies. For environmental science, the current research on greenhouse gas monitoring focuses on the overall carbon cycle and on identification of greenhouse gas fluxes, sources, and sinks [3] (especially for methane, CO_2, and NO_x). Oxygen is also measured with CO_2 to determine biotic respiration rates.

A common method currently used to generate chemical emissions maps is based on self reporting by industry, which does not provide information about natural sources, and is prone to human sources of error. This method has been used for mapping CO_2 emissions in the United States within Project Vulcan [8].

Satellites are used for wide area sensing, but real-time spatial resolution and sensitivity are limited, and deployment costs are exceptionally high. The Orbiting Carbon Observatory [14] was designed specifically for this purpose, but recently failed to achieve orbit.

Another commonly used method to collect emissions source information is based on ultra-high sensitivity instrumentation installed into vehicles (e.g. airplanes, trailer based laboratories), and with data acquired in cross patterns [11, 20]. This method requires operation and

maintenance personnel, with spatial monitoring limited to a point measurement at the current location of the vehicle, and is extremely limited temporally by operational schedules. Additionally, for airborne platforms the sensitivity must be extremely high (ppt level) to detect ground emissions at high altitudes after the gases have diffused considerably from the sources.

There exist field deployed long-term carbon sensing networks deployed to measure long term chemical flux [16], but these sensors are very few in number and sparsely located.

The standard method of achieving real-time continuous spatial resolution is construction of ultra-high sensitivity standoff sensors with area coverage provided by opto-mechanical scanning, which provide only path averaged information with limited spatial resolution and can have infrastructure, maintenance, and line-of-sight issues.

Integration of chemical sensors into WSNs become necessary in monitoring hundreds of sq. km with <0.5 sq. km resolution in such applications as leak detection around geological carbon sequestration sites, industrial and natural emissions (especially methane) monitoring, agricultural monitoring, or volcanic emissions monitoring [19]. Furthermore, application of networks for unauthorized industrial emissions monitoring or implementation of an exact carbon credit trading system (e.g. the successor to the Kyoto Protocol) will require measurement precision, high temporal (second time scales) and spatial resolution capabilities, which are not available with currently available trace-gas monitoring methods.

3. METHODS

3.1 Laser Spectroscopy

We are developing laser spectroscopy based trace-gas sensors. Each molecule exhibits a unique absorption spectrum, which in most cases is well documented in terms of absorption strength vs. frequency, temperature, and pressure in spectroscopic databases [10, 21, 22] . The molecular structure determines at which frequencies the incident light will be absorbed by the molecule. Even molecular species with different isotopic components (isotopologues) can be distinguished with the proper selection of absorption spectral lines and adequate sensitivity [7].

The basic sensor architecture consists of a tunable single frequency laser, a volume of the gas sample, and a photodetector which detects the radiation transmitted through the sample. This architecture is commonly called Tunable Diode Laser Absorption Spectroscopy (TDLAS) [4]. Usually individual molecular gas species require lasers operating at different wavelengths. The modular design of our platform allows for the integration of various types of lasers directly.

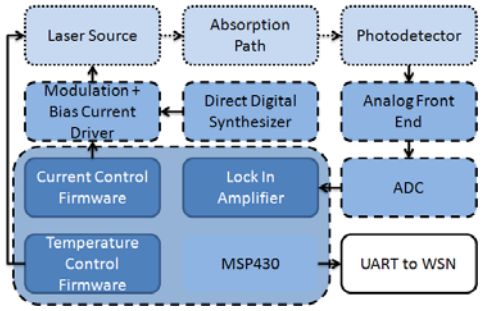

Figure 3: Simplified block diagram of major sensor sub-systems. Blocks with dotted outlines are part of the optical system. Dashed outlines are integrated into the sensor board.

The laser used in our prototype sensor is a Vertical Cavity Surface Emitting Laser (VCSEL, a technology that is used in mass production i.e. laser mice for PCs) operating at wavelength of 766nm. The laser emits single frequency radiation tunable over 10 absorption lines of oxygen via temperature control from -10.0°C to 40°C. The line ${}^{P}Q_{19}(18)$ is targeted with the laser stabilized near room temperature to perform sensitive O_2 spectroscopy.

Mass produced telecom lasers and VCSELs in the 760 nm to 2.7 micron near-IR wavelength region show high Wall-plug Power Efficiency (WPE) and are available at relatively low cost. VCSELs provide 10% WPE, usually producing about 0.5 mW of maximum optical power. Output powers of microwatts can provide sufficient TDLAS spectroscopic information. The excess power allows for sensitivity enhancement methods such as multipass mirror cells, which are lossy due to reflection off non-ideal mirrors. Telecom diode lasers are mass produced in the near-IR for the telecommunications industry, and provide ~7% WPE at 85mW of maximum optical power, but typically run at much lower powers for absorption spectroscopy.

Quantum and Interband Cascade Lasers (QCL, ICL) in the 3-12 micron mid-IR region can target the strongest ro-vibrational molecular absorption bands, thus providing the highest sensitivity typically required for atmospheric applications. These lasers are still under development, but at the current rate of improvement of wall-plug efficiency, spectral quality, and cost, these sources are expected to prove essential in the field of spectroscopic trace-gas sensor networks. Single frequency QCLs suitable for gas sensing typically achieve 1mW optical power with 0.1% WPE at room temperature [2] [5], but offer up to two orders of magnitude better trace-gas concentration sensitivity than the near-IR telecom wavelengths using equivalent sensor parameters.

3.2 Embedded Control and Signal Processing

We have designed the custom embedded control system to perform autonomous laser spectroscopic sensing (see Figure 3). It provides a interface to any mote with a

standard Universal Asynchronous Receiver Transmitter (UART) or Inter-Integrated Circuit (I2C) interface, which presently is configured for direct interface to a Telos [18] communication module.

The embedded system is based on a single 8MHz TI MSP430F1611 system controller. The controller continuously performs a digital 32-bit fixed point PID servo loop at ~1 kHz on the laser temperature to keep the laser stable within 0.001°C. The laser temperature is stabilized using a Peltier thermoelectric cooler module driven by an embedded PWM switched H-bridge for high efficiency.

The laser is driven with an onboard current source with additional sinusoidal modulation at 16 kHz using a reference multiplying Digital-to-Analog Converter (DAC). A 16-bit 200kSPS Analog-to-Digital Converter (ADC) samples a low noise analog front end to the photodetector, and the MSP430 implements real-time lock-in amplifier demodulation. The output low pass filter for the lock-in detection is implemented digitally.

The complete sensor using a VCSEL as the spectroscopic source consumes <0.3W of electrical power. In the following subsections details on the signal processing and embedded systems development will be given.

3.2.1 Automatic Endian Changes

The system power consumption, size, and cost decrease if the internal 12-bit ADC of the MSP430 is used for sampling. However, the dynamic range (the standard measure of lock-in amplifier performance) is directly related to the number of bits, and trace-gas sensing requires the highest dynamic range possible. In this case, the system required high speed digital acquisition of a 16-bit SPI ADC peripheral in order to achieve low noise, high bandwidth, and high dynamic range.

MSP430 is a little-endian processor; unfortunately, most multi-byte SPI peripherals provide big-endian output. The ADC we chose for our lock-in was the 16-bit TI ADS8317 with big-endian output. In one of our preliminary versions of the DSP lock-in firmware, we acquired a buffer of data (720 points of two byte sections = 16-bits of data) in big-endian format, then swapped the bytes in memory as efficiently as possible. Initially we tried to minimize the overhead by 1) performing all of the byte swapping collectively in a single function, 2) using a processor intrinsic swap-bytes function, and 3) unrolling the processing loop 24 times. This method provided adequate performance; however, we determined a more efficient method of data transport to eliminate all byte swapping.

We updated the firmware so the Direct Memory Access (DMA) performed Serial Peripheral Interface (SPI) to memory buffer transfers in reverse order into the buffer (see Figure 4). This changes the endianness of the data automatically; saving 12623 cycles of processing out of

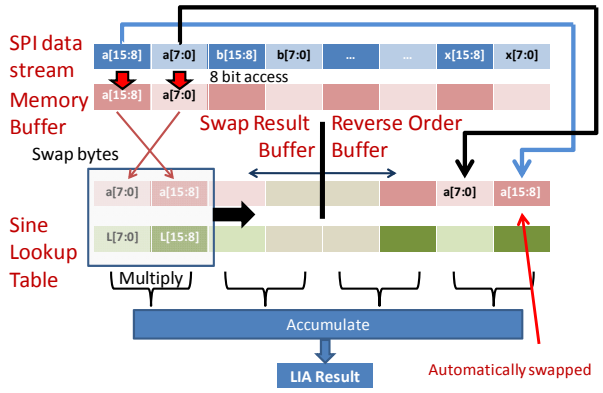

Figure 4: Programming the DMA to acquire SPI byte data to the memory buffer in reverse order eliminates byte swapping time for little-endian processing of our lock-in amplifier.

Table 1: Cycle counts (Rowley compiler) and corresponding maximum loop rates for core functions.

Functionality	MSP430 Cycle Count	Max Loop Rate, 8MHz
PI Digital Controller, 32-bit fixed point	581	13.8kHz
Filter, 64 point 4-pass moving average	774	
Swap bytes (endian change, 720 points, with 24x loop unrolling)	12623	
Lock-in 2 channel, 1 buffer + filter	14003	571Hz
Lock-in 3 channel, 1 buffer + filter	21008	308Hz
Swap + Lock-In 2 channel	26626	300Hz
Swap + Lock-In 3 channel	39249	203Hz
8*16384Hz sampling rate	43956	182Hz

26626 of the original lock-in amplifier algorithm (see Table 1). This allows the MSP430 to sleep, rather than wasting processor cycles to swap the bytes. The overhead saved at 182Hz buffer acquisition rate (8×16384Hz / 720 points) is about 30% of the total 8MHz processing capability.

Thus, only a few changes to buffer pointers and DMA settings were necessary, while providing greater reserve processing capability and/or more idle time. This method can reduce overhead whenever an MSP430 or any other little-endian microcontroller requires a data sourcing serial peripheral of 2 bytes or higher per data point with MSB first (most board level integration serial peripherals) with a serial port only capable of 1 byte per transfer.

3.2.2 Digital Lock-In Amplifier for MSP430

Derivative techniques based on wavelength modulation provide substantial improvement in terms of sensitivity for laser based trace-gas sensing [15]. Demodulation of spectroscopic information is usually performed by Lock-In

Amplification (LIA), which is essentially a homodyne detector coupled with a detection-bandwidth limiting low pass filter.

Digital Signal Processing (DSP) based lock-in amplification is the method of choice in commercial lock-in amplifiers for laboratory use [25]. This method performs local oscillator multiplication and filtering in the digital domain.In order to free up resources to perform DSP lock-in amplification on an 8MHz microcontroller, we used the automatic endian change described in the previous section, coupled with a great deal of optimization to the programming algorithm to achieve high speed synchronous data acquisition and processing on a low power budget. Table 1 lists the processor cycle counts of various functions.

In order to meet real-time processing constraints, we adapted the methods normally used for Finite Impulse Response (FIR) filters [26] on MSP430 into an efficient lock-in technique. This method involved implementing the algorithm around the hardware multiply-accumulate command, hardware integrated timers, and extensive use of DMA.

The method is relatively universal and can be implemented on different platforms. The required components are an SPI port to control reference modulation frequency, 2 timers to synchronously clock the ADC and modulation, and a slave SPI port for the ADC data. We implemented the control systems on the MSP430 processor because it is the same processor family found in many WSN modules such as TelosB/TmoteSky, tinynode, and EyesIFX v2, to name a few [6, 9, 18]. By providing some optimizations we were able to implement high bandwidth performance.

The basic lock-in algorithm is the following: 1) Modulate the laser, 2) Provide analog gain and anti-aliasing filtering for the photodetector signal, 3) Sample the ADC, 4) Multiply the ADC data points by a sine wave in the look-up table with a frequency and phase of interest, 5) low pass filter the mixed signal.

3.2.3 Lock-in amplifier advantages in sensors

A lock-in amplifier is a widely implemented piece of equipment in precision sensors and other measurement systems. Lock-in amplifiers outperform Fast Fourier Transform (FFT) based measurements for single frequency demodulation situations since no processing is wasted outside of the frequency of interest, and the detection bandwidth becomes particularly narrow. The advantages in moving the signal above 1/*f* flicker noise and producing narrow bandwidth detection far outweigh any power or cost concerns for high sensitivity applications similar to trace-gas sensing.

A lock-in amplifier based method is especially useful for laser spectroscopic measurements, because it is capable of two critical functions of the sensor system: laser line-

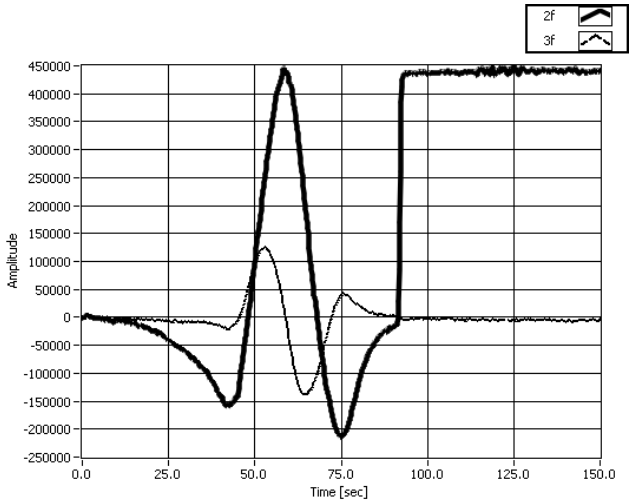

Figure 5: Two channels of the lock-in tuning over an O_2 line. Each channel can change phase or harmonic. The controller locks the line to the 3*f* zero crossing (near 60 seconds) at the 90 second point.

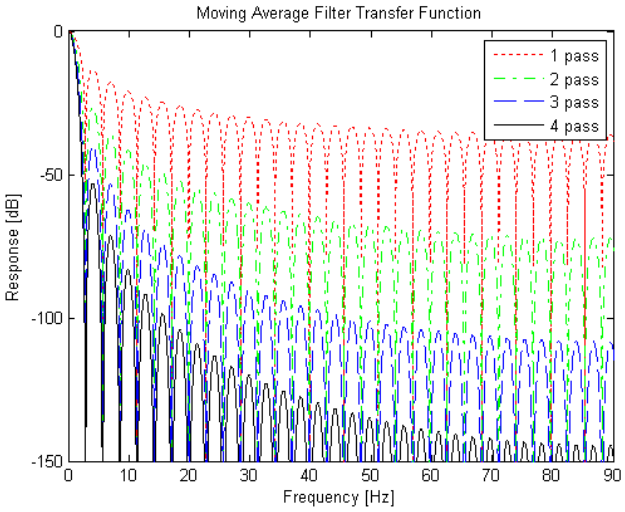

Figure 6: Simulation of a lock-in amplifier digital low pass filter transfer function. Final implementation used a 4-pass moving average filter to keep algorithm loop speed high.

locking (stabilizing the laser output wavelength) to an absorption line, and derivative-based absorption sensing. Line locking can be performed using odd (e.g. 3rd) harmonic of the modulated photodiode signal which resembles the third derivative of an absorption line (absorption lines have Gaussian, Loretzian or Voigt spectral profile), and has a zero-crossing and high slope at the center of the line which is used as an error signal to a PID servo. An absorption measurement can be performed using the 2nd harmonic of the wavelength modulation signal with amplitude directly proportional to concentration, which appears as the second derivative of the absorption signal. An automatic line locking algorithm has been implemented. First the laser temperature is

scanned to acquire the complete spectrum of absorption line, then the center of the line is identified and the laser is locked to it using 3rd harmonic as an error signal (see Figure 5).

Derivative sensing allows for effective suppression of slowly varying baseline changes and drifts, thus improving the overall signal-to-noise ratio of the sensor. Additionally this eliminates the necessity of real-time polynomial least-squares fitting operations for baseline correction, which require a very fast processor for many division operations, due to inversion of matrices, which we explored in Ref. [24]. Additionally, the line-locked signal is probing the region where absorption is the highest. With appropriate code and algorithm optimization we were able to simultaneously provide three channel lock-in detection, with independently addressable phases (at any angle) and/or harmonics in each channel (see Figure 5). Only two channels were possible without the automatic endian change (see Table 1).

Further improvement of the algorithm performance was achieved by combination of the lock-in low pass filter with the output averaging filter. This merges the required processing cycles and allows the use of decimated digital filters to reach long averaging times if it is required by the application.

For standard operation of the sensor, we set a time constant for the 4-pass filter moving average filter to 0.25 seconds to achieve higher stopband rejection compared to 1-3 passes (Figure 6).

3.2.4 Component Systems Performance

In order to evaluate the performance of the low-power DSP lock-in detection we performed a comparison of signal-to noise-ratio measured by our ultra-low power, compact lock-in and a laboratory lock-in amplifier (EG&G Instruments 7265). The reference modulation clock signal from the sensor board was used to synchronize both the internal and the external lock-in. The laser was modulated with 0.165 mA peak-to-peak sinusoidally, biased with 0.91 mA, and held at temperature of 21.00 °C.

The laser radiation passed through two crossed calcite polarizers with extinction ratio of 1.5×10^5:1. The residual amplitude modulation of the laser intensity was detected at 1st harmonic using both lock-ins. For the crossed polarizer the target signal is buried in thermal noise of the photodetector (a silicon photodiode).

The signal amplitude could be varied by rotating the polarizer. The resulting signal-to-noise ratio, calculated using both in-phase and quadrature components is shown in Figure 7.

The result shows that the signal-to-noise ratio measured with our system is similar to the external laboratory lock-in amplifier. The measured signals ranged from ~5 to 26 nA.

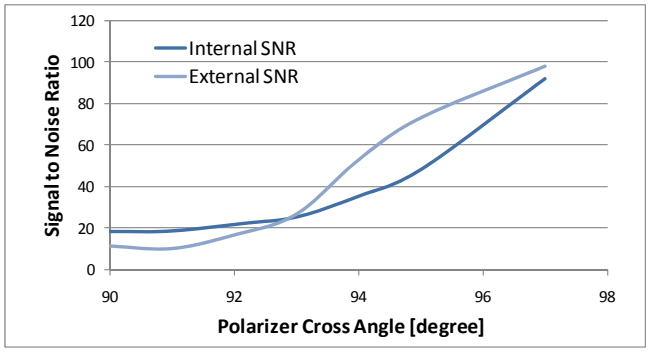

Figure 7: Signal to noise ratio measured with an integrated lock-in amplifier and compared to a laboratory lock-in. The lock-ins extract the modulated laser intensity buried in photodetector thermal noise.

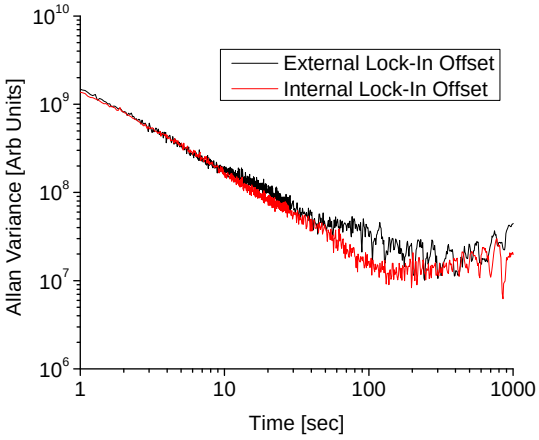

Figure 8: Allan variance plot indicating measured lock-in amplitude versus averaging time for averaging times > 1sec. (the averaging times must be longer than ~3x time constant of the lock-in detection which is 3*0.25sec=0.75sec)

In order to determine whether longer term performance was comparable, a stability test using an Allan variance provides a measurement of system stability (Figure 8). Both systems show similar white (Gaussian) noise limited performance (the range where the slope is -1 on the log-log plot) before drift sets in at ~100 seconds.

Total power budget of 0.0855W for the lock-in amplifier includes ADC (0.004W), analog front end (0.030W), direct digital synthesis (DDS) performed by AD9833 (0.020W), switched capacitor filter based on MAX7422 (0.009W), and the MSP430 processing power of 0.0225W (assuming 48% [21008/43956 total possible cycles], at 3.3V in 8MHz active mode).

The implemented high precision DDS based frequency tuning provides the ability to perform photoacoustic and quartz-enhanced photoacoustic spectroscopy, which requires audio frequency resonance matching of the

acoustic component. However, if the application does not require high precision DDS based frequency tuning, as in direct absorption spectroscopy that we describe in this work, the power consumption can be reduced to 0.0655W.

Additional savings in power can be achieved by lowering the modulation bandwidth, and using lower gain-bandwidth op-amps. However, 1/*f* flicker noise in electronics and photodetectors provides a direct tradeoff.

4. CHEMICAL PLUME DETECTION

As a proof of concept, we have deployed a small sensor network using three O_2 sensors for real-time concentration monitoring. We implemented multipass cells for sensitivity enhancement for a slight increase in the total size of the instrument (18x6x5 cm), but without increasing power consumption. The simulation of the spot pattern in MATLAB and the resulting model in Solidworks are shown in Figure 9. The complete sensor nodes were set up in a triangular configuration a few meters apart. A laptop with a Telos card plugged into the USB port acted as the basestation, and broadcast a command to start measurements simultaneously. The basestation then requested data from each node sequentially. We implemented a LabVIEW interface to receive all of the data and provide visualization. Each sensor transmitted a 30 byte packet (with debugging information) every 0.3 seconds. This provides sensor operational information such as laser temperature, laser current, and lock-in values. However, the bare minimum data output required is a single 32-bit value from the 2*f* lock-in amplifier (while line-locked), which is proportional to concentration.

A short release of oxygen (<5 seconds) from a lecture bottle containing 100% oxygen created a plume while the sensors were running in real-time. Using both time-of-flight and relative quantification, we were able to determine the approximate location of the release soon after, assuming no pressure eddies (See Figure 10). Within LabVIEW, we used MATLAB server to run the localization algorithm using sensor data recorded from our interface. By providing this interface to MATLAB we can allow more complicated transport models and real-time mapping in the future.

Previous sensor networking literature has provided statistical algorithms to determine which nodes in the network should be measuring or communicating in order to conserve overall sensor network energy stores [34]. With trace-gas sensing, changes on large area scales are typically slow and relatively continuous (due to gas diffusion), providing opportunities for these sensors to interpolate data between themselves and turn off nodes which do not provide significant information. This will be critical in laser spectroscopic deployments, since unlike sensors of simple environmental parameters (temperature, pressure etc) these sensors require higher computational and electrical power. In some cases their electrical power consumption directly scales the detection limits which will require more parameters for energy management.

Figure 9: 31 pass multipass cell model in Solidworks designed from mostly off-the-shelf parts.

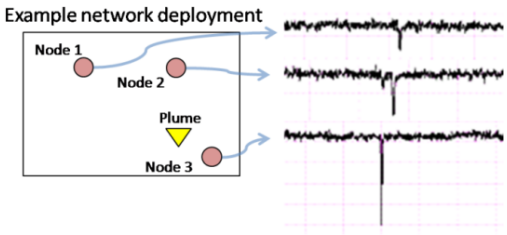

Figure 10: A demonstration deployment of 3-node real-time wireless sensor network measuring an O_2 plume. Data is synchronized and acquired continuously, and the plume could be localized using time-of-flight with nodes ~3 meters apart. The concentration signal is inverted due to the selected phase of the lock-in.

5. CONCLUSIONS

A laser based integrated spectroscopic platform for real-time chemical sensing has been developed from the ground up. A low power, compact, digital lock-in amplifier developed for high precision sensors within WSN frameworks provides the stability and noise levels comparable with those of standalone laboratory equipment (in this particular application). The overall platform provides sensor characteristics required for multi-node distributed environmental monitoring over long periods of time. This instrumentation can target a variety of chemicals using the same architecture, provided the appropriate laser sources and photodetectors are available. Our sensor platform can be directly integrated into a WSN using Telos motes. We believe this technology will be a critical tool for routine wide area chemical sensing for environmental, industrial and security applications.

6. ACKNOWLEDGMENTS

This project was funded by the NSF MIRTHE ERC and NSF MRI Award #0723190. We thank Dr. Barry McManus at Aerodyne Res. Inc. for review of the multipass cell design, and Prof. Andreas Terzis and Razvan Musaloiu-E. at Johns Hopkins University for mote interface assistance.

7. REFERENCES

[1] Akyildiz, I. F., Su, W., Sankarasubramaniam, Y. and Cayirci, E. Wireless sensor networks: a survey. *Computer Networks*, 38, **4**, 393-422, (2002).

[2] Blaser, S., Bachle, A., Jochum, S., Hvozdara, L., *et al.* Low-consumption (below 2W) continuouswave singlemode quantum-cascade lasers grown by metal-organic vapour-phase epitaxy. *Electronics Letters*, 43, **22**, (2007).
[3] Cox, P. M., Betts, R. A., Jones, C. D., Spall, S. A., *et al.* Acceleration of global warming due to carbon-cycle feedbacks in a coupled climate model. *Nature*, 408, **6809**, 184-187, (2000).
[4] Curl, R. F. and Tittel, F. K. Tunable infrared laser spectroscopy. *Annual Reports on the Progress of Chemistry Section "C"*, 98, 219-272, (2002).
[5] Darvish, S. R., Slivken, S., Evans, A., Yu, J. S., *et al.* Room-temperature, high-power, and continuous-wave operation of distributed-feedback quantum-cascade lasers at lambda ~ 9.6 mu m. *Applied Physics Letters*, 88, **20**, 201114-201113, (2006).
[6] Dubois-Ferrière, H., Fabre, L., Meier, R. and Metrailler, P.,2006. TinyNode: a comprehensive platform for wireless sensor network applications. In Proceedings of the 5th international conference on Information processing in sensor networks (Nashville, Tennessee, USA, 2006). ACM, 358-365, DOI=
[7] Durry, G., Joly, L., Le Barbu, T., Parvitte, B., *et al.* Laser diode spectroscopy of the H2O isotopologues in the 2.64 [mu]m region for the in situ monitoring of the Martian atmosphere. *Infrared Physics & Technology*, 51, **3**, 229-235, (2008).
[8] Gurney, K. R., Chen, Y.-H., Maki, T., Kawa, S. R., *et al.* Sensitivity of atmospheric CO2 inversions to seasonal and interannual variations in fossil fuel emissions. *J. Geophys. Res.*, (2005).
[9] Infineon, A., *EYES*, http://www.eyes.eu.org/
[10] Jacquinet-Husson, N., Arie, E., Ballard, J., Barbe, A., *et al.* The 1997 spectroscopic GEISA databank. *Journal of Quantitative Spectroscopy and Radiative Transfer*, 62, 205-254, (1999).
[11] Jiang, M., Marr, L. C., Dunlea, E. J., Herndon, S. C., *et al.* Vehicle fleet emissions of black carbon, polycyclic aromatic hydrocarbons, and other pollutants measured by a mobile laboratory in Mexico City. *Atmospheric Chemistry & Physics*, 5, 3377-3387, (2005).
[12] Laakso, M., Jalonen, M. and Laukkanen, S., *A Compact Ruggedized Tunable Diode Laser Spectrometer for Oxygen Sensing*, http://www.vaisala.com/instruments/products/oxygen/omt355/compact%20ruggedized%20tdl%20spectrometer%20for%20oxygen%20sensing.pdf
[13] Lancaster, D. G., Fried, A., Wert, B., Henry, B., *et al.* Difference-Frequency-Based Tunable Absorption Spectrometer for Detection of Atmospheric Formaldehyde. *Applied Optics*, 39, **24**, 4436-4443, (2000).
[14] NASA, *Orbital Carbon Observatory*, http://oco.jpl.nasa.gov/
[15] Oh, D. B., Paige, M. E. and Bomse, D. S. Frequency Modulation Multiplexing for Simultaneous Detection of Multiple Gases by use of Wavelength Modulation Spectroscopy with Diode Lasers. *Applied Optics*, 37, **12**, 2499-2501, (1998).
[16] Peters, W., Jacobson, A. R., Sweeney, C., Andrews, A. E., *et al.* An atmospheric perspective on North American carbon dioxide exchange: CarbonTracker. *Proceedings of the National Academy of Sciences*, 104, **48**, 18925-18930, (2007).
[17] Petrov, K. P., Waltman, S., Simon, U., Curl, R. F., *et al.* Detection of methane in air using diode-laser pumped difference-frequency generation near 3.2 μm. *Applied Physics B: Lasers and Optics*, 61, **6**, 553-558, (1995).
[18] Polastre, J., Szewczyk, R. and Culler, D.,2005. Telos: enabling ultra-low power wireless research. In Proceedings of the 4th international symposium on Information processing in sensor networks (Los Angeles, California, 2005). IEEE Press, 48-48, DOI= 10.1109/IPSN.2005.1440950.
[19] Richter, D., Erdelyi, M., Curl, R. F., Tittel, F. K., *et al.* Field measurements of volcanic gases using tunable diode laser based mid-infrared and Fourier transform infrared spectrometers. *Optics and Lasers in Engineering*, 37, **2-3**, 171-186, (2002).
[20] Roller, C., Fried, A., Walega, J., Weibring, P., *et al.* Advances in hardware, system diagnostics software, and acquisition procedures for high performance airborne tunable diode laser measurements of formaldehyde. *Applied Physics B: Lasers and Optics*, 82, **2**, 247-264, (2006).
[21] Rothman, L. S., Jacquemart, D., Barbe, A., Chris Benner, D., *et al.* The HITRAN 2004 molecular spectroscopic database. *Journal of Quantitative Spectroscopy and Radiative Transfer*, 96, **2**, 139-204, (2005).
[22] Sharpe, S. W., Johnson, T. J., Sams, R. L., Chu, P. M., *et al.* Gas-Phase Databases for Quantitative Infrared Spectroscopy. *Applied Spectroscopy*, 58, **12**, 1452-1461, (2004).
[23] So, S., Koushanfar, F., Kosterev, A. and Tittel, F.,2007. LaserSPECks:: laser SPECtroscopic trace-gas sensor networks - sensor integration and applications. In Proceedings of the 6th international conference on Information processing in sensor networks (2007). ACM, 226-235, DOI= http://doi.acm.org/10.1145/1236360.1236391.
[24] So, S. G., Wysocki, G., Frantz, J. P. and Tittel, F. K. Development of Digital Signal Processor Controlled Quantum Cascade Laser Based Trace Gas Sensor Technology. *Sensors Journal, IEEE*, 6, **5**, 1057-1067, (2006).
[25] SRS, *Lock In Amplifier - SR830*, http://www.thinksrs.com/products/SR810830.htm
[26] TI, *Digital FIR Filter Design Using the MSP430F16x*, http://focus.ti.com/lit/an/slaa228/slaa228.pdf
[27] Toci, G., Mazzinghi, P., Mielke, B. and Stefanutti, L. An airborne diode laser spectrometer for the simultaneous measurement of H2O and HNO3 content of stratospheric cirrus clouds. *Optics and Lasers in Engineering*, 37, **5**, 459-480, (2002).
[28] Todd, M. W., Provencal, R. A., Owano, T. G., Paldus, B. A., *et al.* Application of mid-infrared cavity-ringdown spectroscopy to trace explosives vapor detection using a broadly tunable (6–8 μm) optical parametric oscillator. *Applied Physics B: Lasers and Optics*, 75, **2**, 367-376, (2002).
[29] Uehara, K. and Tai, H. Remote detection of methane with a 1.66-um diode laser. *Applied Optics*, 31, **6**, 809-814, (1992).
[30] Webster, C. R., Flesch, G. J., Mansour, K., Haberle, R., *et al.* Mars Laser Hygrometer. *Applied Optics*, 43, **22**, 4436-4445, (2004).
[31] Wen, X.-F., Sun, X.-M., Zhang, S.-C., Yu, G.-R., *et al.* Continuous measurement of water vapor D/H and 18O/16O isotope ratios in the atmosphere. *Journal of Hydrology*, 349, **3-4**, 489-500, (2008).
[32] Williams, J., Fischer, H., Hoor, P., Pöschl, U., *et al.* The influence of the tropical rainforest on atmospheric CO and CO2 as measured by aircraft over Surinam, South America. *Chemosphere - Global Change Science*, 3, **2**, 157-170, (2001).
[33] Wysocki, G., Lewicki, R., Huang, X., Curl, R. F., *et al.* Continuous monitoring of nitric oxide at 5.33 mu m with an EC-QCL based Faraday rotation spectrometer: laboratory and field system performance. *Quantum Sensing and Nanophotonic Devices VI, Proc. SPIE*, 7222, **72220M-8**, (2009).
[34] Zhang, H. and Hou, J. Maintaining Sensing Coverage and Connectivity in Large Sensor Networks. *Ad Hoc & Sensor Wireless Networks*, 1, **1-2**, (2005).